JJMIE

Volume 17, Number 2, June. 2023
ISSN 1995-6665
Pages 139 – 154
https://doi.org/10.59038/jjmie/170201

Jordan Journal of Mechanical and Industrial Engineering

CFD Simulation of Energy Transfer within a Membrane Heat Exchanger under Turbulent Flow

Shuruq Shawish [1], Diala Bani Mostafa [2], Rafat Al-Waked [1,*], Mohammad S. Nasif [3]

[1] Department of Mechanical and Maintenance Engineering, German Jordanian University, Amman 11180, Jordan
[2]Mechanical Engineering Department, University of Texas at Tyler, Tyler, Texas 75799, USA
[3]Department of Mechanical Engineering. Universiti Teknologi PETRONAS, Seri Iskandar 32610, Perak, Malaysia

Received 4 Jan 2023 *Accepted 18 Apr 2023*

Abstract

Air-to-air fixed plate enthalpy membrane exchanger is considered one of the equipment used in energy recovery services. Thermal performance of air-to-air energy recovery ventilator is examined numerically using a 3D CFD simulation. Air flow inside the exchanger is tested using four numerical turbulence models: Standard k-ε, k-ε renormalization group (RNG), k-ε realizable and k-ω shear-stress transport (SST) models. The adopted heat and mass exchange element within the ventilator (membrane) is a thin 98 μm porous 60 gsm Kraft paper. A user defined function (UDF) has been developed to enable the CFD model to estimate amounts of mass exchanged between the two sides of the membrane. Grid dependency study is conducted and results have shown that a perpendicular distance of 50 μm or less from the membrane surface would result in a negligible variation in the ERV thermal effectiveness. The validated CFD model and UDF code against experimental measurement resulted in a maximum difference in thermal effectiveness of 3.6%. Results have shown that the SST k-ω turbulence models under enhanced wall treatment showed more sensitivity to flow at all Re values when compared with the k-ε simulated models.

Keywords: CFD; ERV; heat transfer; mass transfer; turbulence; energy recovery.

Nomenclature

C_p	*Specific heat* (J kg^{-1} K^{-1})
C_h	*Flow channel height* (m)
D	*Air or moisture diffusion coefficient* (m^2 s^{-1})
E	*Mechanical Energy* (J kg^{-1})
G	*generation function*
h	*Enthalpy* (J kg^{-1})
H	*Total Enthalpy* (J kg^{-1})
h_{fg}	*Enthalpy of evaporation* (J kg^{-1})
J	*Diffusion flux* (kg m^{-2})
K	*Thermal conductivity* (W m^{-1} K^{-1})
k	*Turbulent kinetic energy* (m^2 s^{-2})
M_w	*Molecular weight* (kg mol^{-1})
$\dot{m}$	*Mass flow rate* (kg s^{-1})
P	*Pressure* (Pa)
P_{op}	*Operating pressure* (Pa)
q_h	*Sensible heat flux* (W m^{-2})
R	*Universal gas constant* (J K^{-1} mol^{-1})
Sc	*Schmidt Number*
S_ϕ	*Source term*
T	*Air temperature* (K)
V, U	*Flow velocity* (m s^{-1})
x, y, z	*Cartesian coordinates*
Y_i	*Air or moisture mass fraction* (kg kg^{-1})
y^+, y^*	*Non dimensi onal parameters.*

Greek letters

$\sigma_\varepsilon, \sigma_k$	*Inverse effective Prandtl number*
ΔP	*pressure drop* (Pa)
ΔTR	*Temperature difference ratio*
δ	*Thickness* (μm)
ε	*Effectiveness* (%)
ε	*turbulent kinetic energy dissipation rate* (m^2 s^{-3})
Γ_ϕ	*Diffusion coefficient of quantity* ϕ
ρ	*Density* (kg m^{-3})
ϕ	*Variable quantity (1, U, V, W, T, Y_v)*
τ_{ij}	*Deviatoric stress tensor* (Pa)
μ	*Viscosity* (Pa.s)
ω	*Humidity ratio* (kg kg^{-1})
ω	*Specific dissipation rate* (s^{-1})

Subscripts

ci	*cold air at inlet*
co	*cold air at outlet*
cs	*cold membrane side*
h	*hot*
hi	*hot air at inlet*
ho	*hot air at outlet*
hs	*hotmembrane side*
m	*membrane*
ma	*mixed air*
mc	*membrane cold surface*
mh	*membrane hot surface*
t	*turbulent*

1. Introduction

The goal to lower greenhouse gas emissions and to make buildings fulfill strict performance and comfort standards, the combination of energy recovery and energy-efficient

* Corresponding author e-mail: Rafat.Alwaked@gju.edu.jo.

technologies could be seen as a potential strategy [1, 2]. Energy consumption, indoor air quality and thermal comfort are issues that arise when designing air conditioning systems[3, 4]. One way to reducing energy consumption and increasing indoor air quality while maintaining thermal comfort is the use of 100% fresh outdoor air in cooling systems integrated with energy recovery unit. Fixed plate membrane heat exchangers or energy recovery ventilators (ERV) is considered a high potential technology that could be utilized in modern energy efficient buildings [5].

A typical ERV consists of a plastic frame that fixed a membrane or a Kraft paper in-between similar to the one shown by Figure 1. The energy recovery process inside the an air-to-air ERV is shown in more details by Figure 2. The hot/humid side (the regeneration airstream) has higher level of energy that would be transferred to the membrane surface via convection. This energy is conducted (heat) and diffused (mass) through the membrane. The cold/less humid stream side (the process airstream) which has a lower level of energy absorbs the transferred energy via convection. Consequently, the hot/humid air is transformed into a cooler and less humid air before it enters the cooling coiled of the system at relatively low energy cost.

According to ASHRAE [6], air speed of 5 m/s could be reached inside a given ERV. The distance between two membranes inside the ERV could be greater than 2.5 mm that causes a flow of turbulent nature at 5 m/s air speed. The impact of obstacles resulted from the plastic frame within the heat exchanger plays a major role into enhancing heat transfer and creating turbulence [7]. Selection of any of the available turbulence models for CFD simulations differs from one researcher to another. The usage of a turbulence model would depend on: geometry of the model, how complex the problem is and how accurate the result is required.

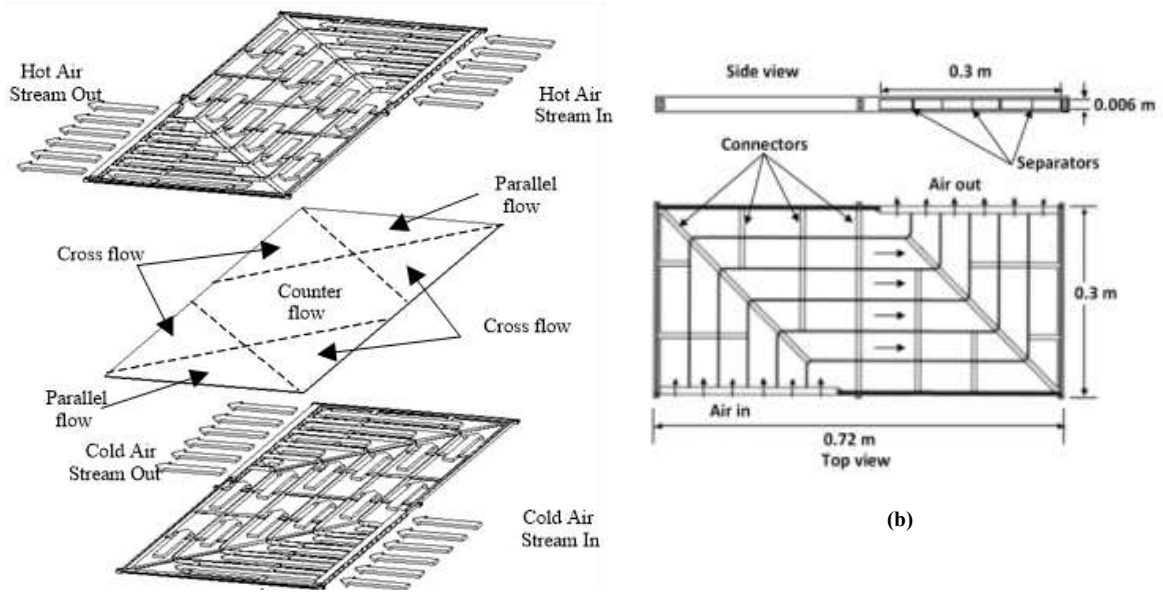

Figure 1. Details of the simulated fixed plate ERV: (a) channel structure, (b) Connectors and separators.

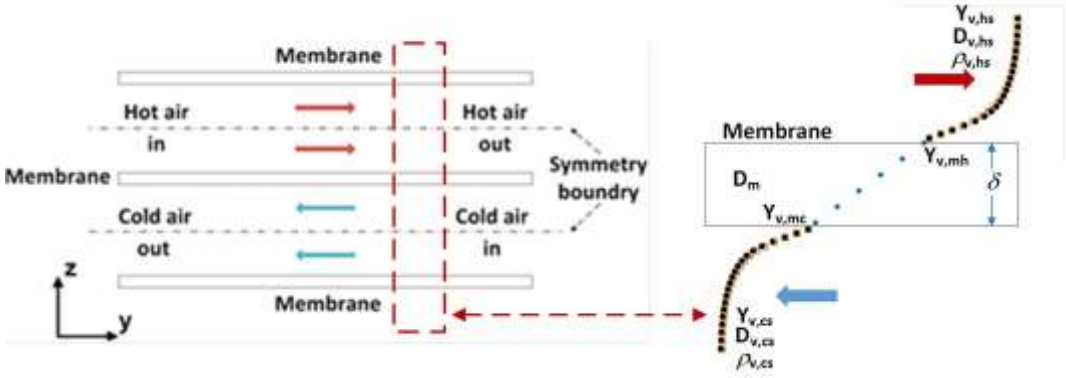

Figure 2. Modelling of mass transfer across the simulated membrane.

In CFD packages, a wide range of turbulence models are available and the most widely used model for heat exchanger design optimization is the k- ε turbulence model[8, 9]. Gawande et al. [10] reported that the RNG k-ε model was preferable to simulate turbulent flow inside a smooth solar air channel when compared with Realizable k-ε, Standard k- ε and SST k-ω turbulence models. Kumar et al. [11] preferred the RNG k- ε turbulent model in their

investigation of turbulent flow inside various types of finned tubes. Shabanian et al. [12] employed the RNG k- ε turbulent model to study an air cooled heat exchanger with different types of tube inserts in relation to its thermal performance. Li et al. [13] utilized the realizable k-εturbulence model to simulate the turbulent flow within an enhanced tube in tube heat exchanger. Ozden and Tari [14] reported that realizable k- ε outperformed standard k- ε and Spalart–Allmaras turbulence models in simulating the turbulent flow inside their shell and tube heat exchanger.

The shear stress transport (SST) k-ω turbulence model has also been considered one of the best turbulence model in Ansys® Fluent v18.1 for the prediction of friction characteristics in rough rectangular ducts in addition to the prediction of heat transfer. Chaube et al. [15] adopted the SST k-ω turbulence model to simulate a solar air heater with different roughness elements. Pal et al. [16] reported that standard k- ε and SST k-ω models produced close agreement with experimental results. The SST k-ω required more mesh elements than the standard k- ε model which resulted in longer computation times. Hatami et al. [17] reported that the SST k-ω and RNG k- ε turbulence models produced similar acceptable results in their double pipe heat exchanger CFD simulations. Sharma and Kalamkar [18] reported that the SST k-ω and RNG k- ε models are the widely used turbulence models for simulating turbulent flow inside a ribbed duct and found good agreement with experimental measurements. Researchers have acknowledged the accuracy of SST k-ω turbulence model in predicting heat-transfer and pressure-drop performance of finned-tube bundles in cross flow[19] and of compact heat exchangers made of corrugated plates [20].

In summary, researchers have concluded that the SST k-ω and RNG k- ε models are the most adopted turbulence models in simulating turbulent flow inside a ribbed duct when compared to experimental results[18]. These investigations, so far, were mainly about sensible heat transfer across walls of pipes/ducts of different heat exchangers.

CFD simulations of heat and/or mass transfer within membrane heat exchangers have been conducted and results were reported [21-28]. These investigations were different in their natures: energy recovery or heat recovery simulation. The energy recovery process depends on the resulted energy transfer through the investigated membrane [29-32]with different flow configuration: hybrid flow [33-36], Counter [37, 38], cross flow [39], parallel flow [40], two dimensional CFD model of parallel flow [41]. The heat recovery process is based on heat transfer process only [42]. The common factor among these CFD simulations is the adoption of laminar flow strategy for energy transfer analysis.

Simulation of turbulent flow inside fixed plate ERVs to model energy transfer that consists of combined heat and moisture has not been fully examined, yet. Moreover, many research opportunities for understanding the nature of mass transfer across membranes using complex spacer geometries do still exist.

In this paper, different turbulence models were examined and their effects on the membrane heat exchanger performance were analyzed: Standard k-ε, RNG k-ε, realizable k-ε and SST k-ω models. A user-defined-function (UDF) was developed and incorporated into Ansys® Fluent v18.1 CFD software to accommodate mass transfer modelling across variable resistance 60 gsm Kraft paper membrane. Effects of different mesh sizes on the accuracy of simulations were also examined. The validated CFD code was then used to examine effects of ambient weather conditions and variable flow rates of the thermal performance. Findings in this paper are useful for researchers who perform membrane heat exchanger modelling giving the fact that choosing the right turbulent model is very important in ensuring the accuracy of the results. A case study is utilized to show the advantage of adopting ERV unit on HVAC energy consumption, CO_2 emissions and financial savings.

2. Simulation Details

The Z-Shape heat exchanger flow channels consisted of 98 plastic flow channels. The plastic channels were assembled together so that the cold air stream channel is laterally inverted from the hot air stream channel. Each flow path channel is made of plastic and consist of five flow separators the reason of having flow separators is to obtain more uniform flow distribution over the heat transfer surface. Since the 60 gsm Kraft paper is placed between the flow frames, the Z-flow separators will also contribute to holding firmly the 60 gsm Kraft paper heat transfer surface. This Z-shaped flow configuration provides a counter flow profile over substantial part of the membrane surface. As a result, heat and moisture transfer will increase relative to the increase in the counter flow profile over a large part of the membrane surface.

The current fixed plate ERV model with two half-channels separated by a membrane, shown by Figure 2, were simulated using a three-dimensional (3D) double precision CFD model. The exchange processes across the membrane of heat and mass were simulated using the pressure-based solver of Ansys® Fluent v18.1 with the aid of a specially designed UDF under steady-state conditions.It has been assumed that a dynamic equilibrium does exist for the H_2O vapor adsorption and desorption across the membrane with the equal heat of vaporization and heat of sorption of constant values. Furthermore, the variable mass transfer resistance of the 60 gsm Kraft paper was adopted within the UDF. It is worth mentioning that turbulent flow conditions do exist inside the ERV. This is due to flow disturbed nature and generated vortices around channel separators and connectors within the simulated ERV.

The discretization of Equations (1)-(3) was achieved based on MUSCAL scheme which is a third order accurate model. Within the pressure-based model, pressure requires external scheme to solve for pressure across the numerical field. Therefore, the SIMPLE algorithm was utilized to link pressure to velocity and define the pressure across the numerical field in link with velocity and consequently with other simulated parameters.

2.1. Governing Equations

The well-known Navier-Stokes, Energy and continuity nonlinear differential equations that describe the incompressible steady-state airflow were written in general form equations as defined by Equation (1) – Equation (3):

$$\nabla.\left(\rho\phi\vec{V}\right)=\nabla.\left(\Gamma_{\phi}\nabla\phi\right)+S_{\phi} \quad (1)$$

$$\nabla\cdot\left(\vec{V}\left(\rho E+p\right)\right)=\nabla\cdot\left(k_{eff}\nabla T-\sum_{i}h_{i}\vec{J}_{i}+\left(\left(\tau_{ij}\right)_{eff}\cdot\vec{V}\right)\right) \quad (2)$$

$$\nabla.\left(\rho\vec{V}Y_{i}\right)=\nabla.\ \vec{J}_{i} \quad (3)$$

Heat transfer due to conduction, energy transfer due to diffusion and viscous heating are presented by the right-hand side of Equation (2), respectively. Full buoyancy effects have been taken into consideration, too.

The mechanical energy *E* and the sensible enthalpy *h* were defined in Equation (4) – Equation (6) as:

$$E=h-\frac{p}{\rho}+\frac{V^{2}}{2} \quad (4)$$

$$h=\sum_{i}Y_{i}h_{i}+\frac{p}{\rho} \quad (5)$$

$$h_{i}=\int_{T_{ref}}^{T}c_{p,i}dT \quad (6)$$

The air or vapor diffusion flux under laminar flow and under turbulent flow was defined according to Equation (7) and Equation (8), respectively.

$$\vec{J}_{i}=-\rho D_{i,ma}\nabla Y_{i} \quad (7)$$

$$\vec{J}_{i}=-\left(\rho D_{i,ma}+\frac{\mu_{t}}{Sc_{t}}\right)\nabla Y_{i} \quad (8)$$

$$Sc_{t}=\frac{\mu_{t}}{\rho D_{t}} \quad (9)$$

$$D_{a,ma}=D_{v,ma}=1.87\times10^{-10}\frac{T^{2.072}}{P} \quad (10)$$

$$\rho=\frac{P_{op}}{RT\sum\frac{Y_{i}}{M_{w,i}}} \quad (11)$$

It should be noted that air and vapor thermodynamic properties including conductivity, specific heat, and viscosity, were function of air temperature[43].

2.1.1. Membrane Modelling

Each flow path channel is made of plastic and consists of five flow separators to obtain more uniform flow distribution over the heat transfer surface. The isotropic steady-state heat and mass transfer processes across the membrane of 98 μm thickness (δ) is defined as [44]:

$$\frac{\partial^{2}T_{m}}{\partial z^{2}}=0 \quad (12)$$

$$\frac{\partial^{2}Y_{i,m}}{\partial z^{2}}=0 \quad (13)$$

Fick's law [44], defined by Equation (14), is used to define the mass flux of H_2O vapor at the surface of the porous 60gsm Kraft paper that is used as a membrane. The more pores in the membrane the higher the moisture is transferred across it, because there will be more paths for the moisture to be transferred through the pores. Moisture transfer across the paper is also affected by the paper micro structure and thickness.

$$j_{v}=-\rho D_{v,ma}\left.\frac{\partial Y_{v}}{\partial z}\right|_{hs}=-\rho D_{m}\left.\frac{\partial Y_{v,m}}{\partial z}\right|_{m}=-\rho D_{v,ma}\left.\frac{\partial Y_{v}}{\partial z}\right|_{cs} \quad (14)$$

Equation (14) across the membrane was solved within the adopted UDF to provide the value of vapor mass flux on both surfaces of the membrane as defended by Equations (15) and (16). Effects of mesh center distances from membrane surface, geometrical, air temperature/moisture and other properties of the membrane as listed in Table 1were embedded in the constants a_1 and a_2. These constants are the result of accumulative mathematical terms within the utilized UDF.

$$Y_{v,mc}=Y_{v,cs}+a_{1}Y_{v,hs}-a_{1}Y_{v,mh} \quad (15)$$

$$Y_{v,mh}=\frac{Y_{v,cs}+\left(a_{1}+a_{2}\right)Y_{v,hs}}{\left(a_{1}+a_{2}+1.0\right)} \quad (16)$$

The ERV sensible (ε_s), latent (ε_l) and total (ε_t) effectiveness were determined from [21]:

$$\varepsilon_{s}=\frac{\dot{m}_{h}c_{p}(T_{hi}-T_{ho})+\dot{m}_{c}c_{p}(T_{co}-T_{ci})}{2\dot{m}_{min}c_{p}(T_{hi}-T_{ci})} \quad (17)$$

$$\varepsilon_{l}=\frac{\dot{m}_{h}h_{fg}(\omega_{hi}-\omega_{ho})+\dot{m}_{c}h_{fg}(\omega_{co}-\omega_{ci})}{2\dot{m}_{min}h_{fg}(\omega_{hi}-\omega_{ci})} \quad (18)$$

$$\varepsilon_{t}=\frac{\dot{m}_{h}(H_{hi}-H_{ho})+\dot{m}_{c}(H_{co}-H_{ci})}{2\dot{m}_{min}(H_{hi}-H_{ci})} \quad (19)$$

The HVAC system performance was based on the annual energy recovered by the ERV in accordance with the air-conditioning, heating and refrigeration institute (AHRI). The recovery efficiency ratio (RER) was adopted to present the ratio of net conditioning energy recovered by the ERV divided by the additional total electric power resulted from the installation of the ERV to achieve that recovery as defined by Equation (20). In the case of air-to-air ERV, the additional electrical power is the power resulted from installing/increasing the capacity of supply ($P_{sf,w\ ERV}$) and exhaust fans ($P_{ef,w\ ERV}$).

$$RER=\frac{\varepsilon_{t}\dot{m}_{min}(H_{hi}-H_{ci})}{\left(P_{sf,w\ ERV}-P_{sf,wo\ ERV}\right)+\left(P_{ef,w\ ERV}-P_{ef,wo\ ERV}\right)} \quad (20)$$

Table 1. Reference values used in simulating membrane based ERV [21].

Property	Value
# of channels	98
Thickness (δ)	98 μm
Channel height (C_h)	6 mm
60 gsm Kraft paper resistance of moisture transfer (R_{60gsm})	(84988 $\Delta\omega$+38.388) m^2.s/kg
Porosity	0.0029
Thermal conductivity	0.12 W/m.K
Heat capacity	871 J/kg.K
Density	613 kg/m^3

2.1.2. Turbulence Models

The two equations models are the most popular turbulence models adopted by the commercial CFD packages. Launder and Spalding [45] have presented the original version of the k-ε model. A two equations model to calculate the turbulence kinetic energy (k) and its rate of dissipation (ε):

$$\frac{\partial}{\partial x_i}\left(\rho k u_i\right)=\frac{\partial}{\partial x_j}\left[\left(\mu+\frac{\mu_t}{\sigma_k}\right)\frac{\partial k}{\partial x_j}\right]+G_k+G_b-\rho\varepsilon \quad (21)$$

$$\frac{\partial}{\partial x_i}\left(\rho\varepsilon u_i\right)=\frac{\partial}{\partial x_j}\left[\left(\mu+\frac{\mu_t}{\sigma_\varepsilon}\right)\frac{\partial \varepsilon}{\partial x_j}\right]+C_{1\varepsilon}\frac{\varepsilon}{k}\left(G_k+C_{3\varepsilon}G_b\right)-C_{2\varepsilon}\rho\frac{\varepsilon^2}{k} \quad (22)$$

where (G_k) and (G_b) are the turbulence generation due to: mean velocity gradients and buoyancy, respectively. The default values of the model constants are [45]:

$C_{1\varepsilon}$ = 1.44 $C_{2\varepsilon}$ = 1.92 C_μ= 0.09 σ_k=1.0 σ_ε= 1.3

The second version of the k-ε model is the renormalization group (RNG)-based k-ε turbulence model which was derived using the RNG mathematical technique based on the instantaneous Navier-Stokes equations [46]:

$$\frac{\partial}{\partial x_i}\left(\rho k u_i\right)=\frac{\partial}{\partial x_j}\left(\alpha_k\mu_{eff}\frac{\partial k}{\partial x_j}\right)+G_k+G_b-\rho\varepsilon \quad (23)$$

$$\frac{\partial}{\partial x_i}\left(\rho\varepsilon u_i\right)=\frac{\partial}{\partial x_j}\left(\alpha_\varepsilon\mu_{eff}\frac{\partial k}{\partial x_j}\right)+C_{1\varepsilon}\frac{\varepsilon}{k}\left(G_k+C_{3\varepsilon}G_b\right)-C_{2\varepsilon}\rho\frac{\varepsilon^2}{k}-R_\varepsilon \quad (24)$$

where α_k and α_ε are the inverse effective Prandtl numbers. Model constants have values derived analytically by the RNG theory:

$C_{1\varepsilon}$= 1.42 $C_{2\varepsilon}$= 1.68

The third version of the k-ε model is the realizable k-ε model were the modeled transport equations for *k* and *ε* are [47]:

$$\frac{\partial}{\partial x_i}\left(\rho k u_i\right)=\frac{\partial}{\partial x_j}\left[\left(\mu+\frac{\mu_t}{\sigma_k}\right)\frac{\partial k}{\partial x_j}\right]+G_k+G_b-\rho\varepsilon \quad (25)$$

$$\frac{\partial}{\partial x_i}\left(\rho\varepsilon u_i\right)=\frac{\partial}{\partial x_j}\left[\left(\mu+\frac{\mu_t}{\sigma_\varepsilon}\right)\frac{\partial \varepsilon}{\partial x_j}\right]+\rho C_1 S\varepsilon-\rho C_2\frac{\varepsilon^2}{k+\sqrt{\nu\varepsilon}}+C_{1\varepsilon}\frac{\varepsilon}{k}C_{3\varepsilon}G_b \quad (26)$$

The model constants are:

$C_{1\varepsilon}$= 1.44 C_2= 1.9 σ_k= 1.0 σ_ε= 1.2.

The shear-stress transport (SST) k-ω model, was developed to predict with good accuracy the flow separation that occurred around smooth surfaces similar to the current simulation[48]:

$$\frac{\partial}{\partial x_i}\left(\rho k u_i\right)=\frac{\partial}{\partial x_j}\left[\Gamma_k\frac{\partial k}{\partial x_j}\right]+G_k \quad (27)$$

$$\frac{\partial}{\partial x_i}\left(\rho\omega u_j\right)=\frac{\partial}{\partial x_j}\left[\Gamma_\omega\frac{\partial \omega}{\partial x_j}\right]+G_\omega+D_\omega \quad (28)$$

where G_k is the turbulence kinetic energy generation due to gradients in mean velocity, G_b represents ω generation, the effective diffusivity of *k* and $\omega$are represented byΓ_k and Γ_ω , respectively, and D_ω represents the cross-species diffusion term.

2.1.3. Turbulence Treatment at Wall

The near wall region could be subdivided into three layers based on the value of the non-dimensional parameters y^+(non-dimensional mesh height nearby walls based on wall shear stress) and/or y^*(non-dimensional mesh height nearby walls based on turbulent kinetic energy) that are defined by Equation (29) and Equation (30):

- Viscous sub layer (y^+< 5): the innermost layer where the flow is near laminar where the molecular viscosity is the main parameter in heat or mass transfer, and momentum.
- Buffer/Blending region (5 < y^+< 60): located between the viscous and fully-turbulent layers. Both of these layers are equally important in this region.
- Fully-Turbulent layer (y^+> 60): it is the outer layer where turbulence is the dominant factor.

$$y^+=\frac{\rho\, u_\tau y_p}{\mu}=\frac{\rho\sqrt{\tau_w/\rho_w}\; y_p}{\mu} \quad (29)$$

$$y^*=\frac{\rho\, C_\mu^{1/4}\, k_p^{1/2}\, y_p}{\mu} \quad (30)$$

where u_τ is the frictional velocity, y_p is the distance from a given near wall point (p) to the wall (w), k_p is the turbulence kinetic energy at point (p).

In order to model the near wall region, two approaches could be adopted:

- Wall functions: they are semi-empirical formulas valid for high Re applications. They are used to link the laminar region from wall and fully turbulent regions.
- Modified turbulence models: they resolve the laminar region near the wall with a given fine mesh. This leads to the use of formulations that are independent of wall dimensionless distance (y^+). These formulations are the default for all ω-equation-based turbulence models and for the ε-equation-based models when the enhanced wall treatment (EWT) is used. If the mesh near thewall is sufficiently fine (the first node near the wall is placed at $y^+\approx1$), then the enhanced wall treatment will be identical to the traditional two-layer zonal model. Therefore, when the mesh nearby the membrane results in y^+< 5, the stress-strain relationship of laminar flow is applied leading to a linear profile of species mass fraction and/or wall temperature.

2.2. Boundary Conditions

The specific boundary conditions of the current simulations were:

- The velocity boundary condition at the ERV hot and cold inlets. Turbulence inputs were turbulence intensity (5%) and hydraulic diameter (0.012 m).
- The pressure outlet condition at the ERV hot and cold outlets.
- For heat exchanger solid surfaces apart from the membrane, no-slip wall boundary condition was used. Within the enhanced wall treatment, the thermal effect option was activated for the investigated k-ε turbulence models. Moreover, the transitional flows and viscous heating effects were activated for the SST k-ω model.
- For hot and cold air steams half of each stream was modelled and symmetry boundary conditions was utilized at center of the steams.

3. Results and Analysis

This section consists of two major parts: ERV effectiveness analysis via a CFD study including its

validation and mesh sensitivity and effects of ERV utilization ferocities in the MENA region climate zone at different flow rates.

3.1. Mesh Dependency

The investigated hybrid flow Z-shape ERV utilized hybrid meshed which was mostly structured mesh elements as shown by Figure 3. Seven cases were investigated to demonstrate effects of mesh distributions on the ERV performance and the validity of the adopted linear laminar profile at the membrane surfaces. The main variation between these cases was the number of elements perpendicular to the membrane surface while maintaining the lateral mesh dimensions at constant number for all the studied cases. The adopted lateral mesh was fine enough to minimize any variation in the results.

The assumption of a linear mass fraction profile is deemed to be valid when $y^+<5$ and/or$y^*<11$. Figure 4 shows that averaged values obtained from both the standard k-ε with the enhanced wall function and the SST k-ω turbulence models were similar. Averaged values of y^+ ranged between 0.36 and 1.82 at face velocity of 0.76 m/s and between 0.98 and 5.22 at face velocity of 2.9 m/s. Similar results were obtained for y*. As expected, the perpendicular distance from the membrane surfaces has a proportional effect of the value of y^+ and y^*. Slight differences were seen in the resulting maximum values at high values of the perpendicular distance. It can be seen that y^+ showed more sensitivity to the adopted turbulence model than y^*.

Mesh element size at membrane sides and separators was not uniformly distributed. As detailed by Figure 5, the high values shown were located nearby the separators. This left most of membrane surface with values of y^+ and y^* in the vicinity of the reported averaged values. All cases complied with the condition of average value of $y^*< 11$. However, the condition of $y^+\approx1$ was met by those cases with perpendicular distances of less than 75 µm. The lowest value of y^+ was found when 25 µm perpendicular distance was used and resulted in aspect ratio value of 60 which might lead to questionable accuracy of the simulation results.

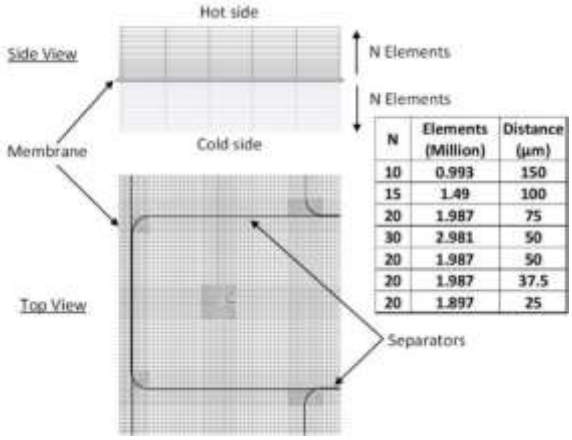

N	Elements (Million)	Distance (µm)
10	0.993	150
15	1.49	100
20	1.987	75
30	2.981	50
20	1.987	50
20	1.987	37.5
20	1.897	25

Figure 3. perpendicular distances of mesh elements used in the CFD model.

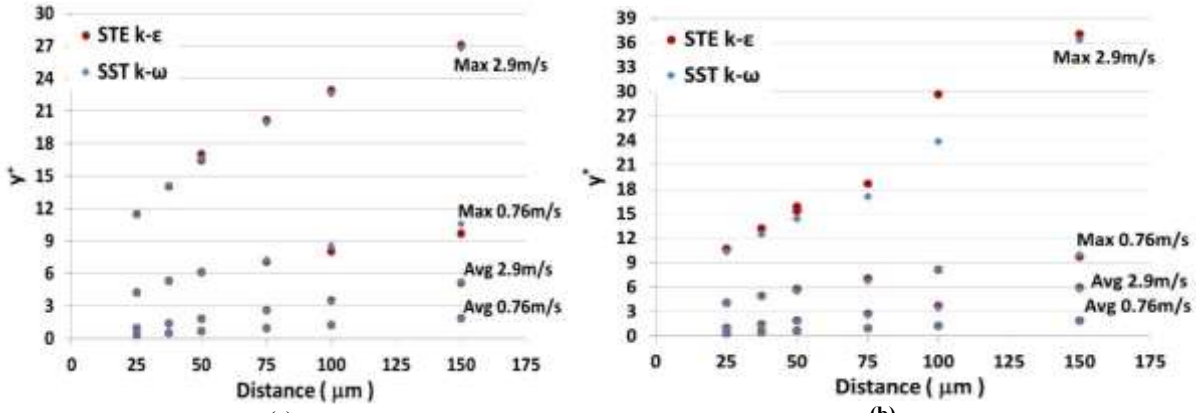

Figure 4. Effect of perpendicular distance and face velocities for the STE k-ε and the SST k-ω turbulence models on the non-dimensional parameters: (a) y^+ value, (b) y* value.

Similar results were obtained from the effectiveness behavior at different meshes as shown by Figure 6. It can be seen that effect of mesh sizes on effectiveness gets more significant as the face velocity increases. Differences in the effectiveness ranged from 0.8% for latent effectiveness and 1.4% for sensible effectiveness at face velocity of 0.76 m/s. These values have increased to 3.5% for latent and 5.0% for sensible effectiveness at face velocity of 2.9 m/s. the resulted number of mesh elements ranged from 0.994 – 2.981 million elements. Four different cases were simulated at a mesh size of 1,987,000 elements and the reported results were different because of the different perpendicular distant of the mesh center from the membrane. Furthermore, it has been reported that fine mesh could produce more accurate results [35, 36]. The effectiveness at the 2.981 million elements case was higher by 0.1% than the 1.987 million elements case. The two cases had the same perpendicular distance. This difference was overcome by reducing the distance to 50 µm with 1.987 million elements case. Consequently, the current study was based on a perpendicular distance of 50 µm and considered to be the standard case.

3.2. CFD Validation Using Different Turbulence Modelling

Dependency of y^+ and/ory^* on the face velocity was examined under four turbulence models with enhanced wall treatment option activated: laminar model, Standard k-ε (STE k-ε), RNG k-ε (RNE k-ε), realizable k-ε (REE k-ε) and SST k-ω. For all the investigated face velocities, Figure 7 shows that the average value for $y^+$was less than 2 and was higher than 11 for y* when face velocities exceeded 2.5 m/s. For these cases, the enhanced wall treatment (k-ε) and the transitional flow (SST k-ω) options become essential for the same reasons stated earlier. Furthermore, the dependence of y+ and y* values on face velocity followed similar trends for the investigated turbulence models. This could be due to the relatively low Re values (Re<5000) where the separation and circulation effects on the turbulent flow were not strong enough to cause major differences. Therefore, results presented by Figure 7 were considered acceptable for the validation purpose of the current CFD code knowing that the membrane (60gsm Kraft paper) surface was exposed to a lower y^+ value.

The experimental results of 60 gsm Kraft paper based ERVreported byNasif [23]were used to validate the developed CFD model. Figure 8 shows that using laminar flow model showed slight differences from the k-ε models with similar trends. An error margin from 1.49% to 2.23% on sensible energy balance and from 0.94% to 3.39% on the latent energy balance between hot and cold streams were reported. At face velocity of 0.76 m/s, an uncertainty in sensible energy of 7.9% and latent energy of 6.0% were reported. At face velocity of 2.9 m/s, an uncertainty in sensible energy of 8.5% and latent energy of 8.2% were reported, too. The comparison of results from the current CFD simulations and the reported ones from Nasif [23] confirms a close match for all turbulence models with 3.6% being the biggest difference.

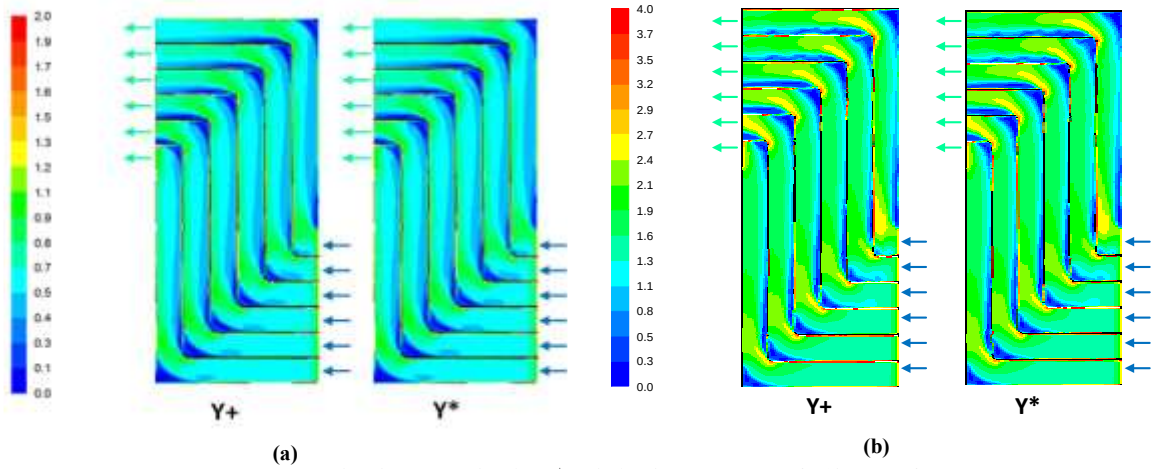

Figure 5. Colored contours showing y^+ and y* values: (a) 0.76 m/s, (b) 2.9 m/s.

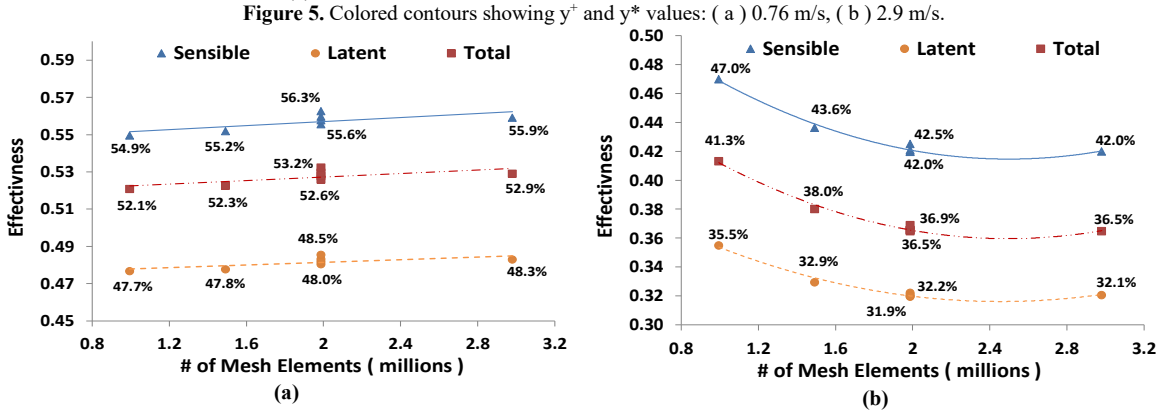

Figure 6. Effectiveness dependance on perpendicular distance effect of the 60 gsm Kraft paper ERV under the SST k-ω turbulence model at different face velocities (a) 0.76 m/s; (b) 2.9 m/s.

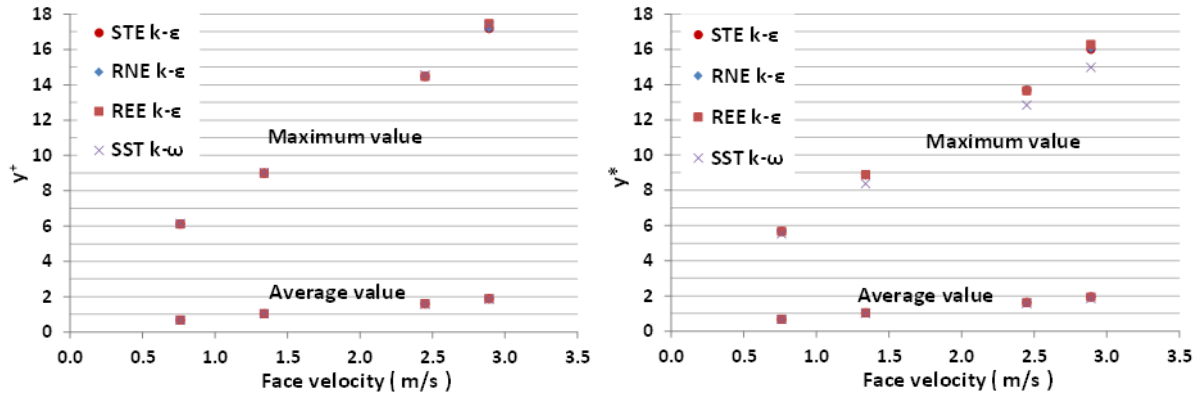

(a) (b)

Figure 7. Effect of face velocity on: (a) y^+ value, (b) y* value.

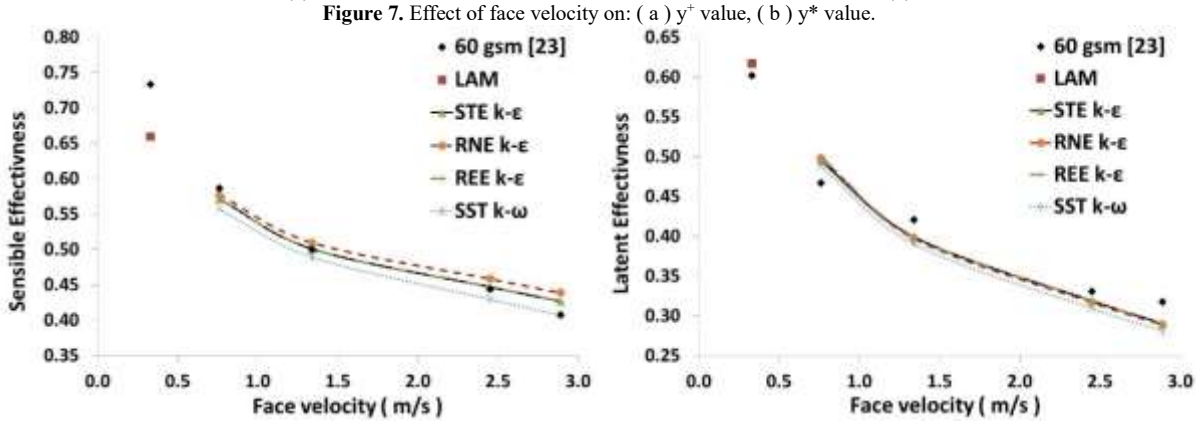

(a) (b)

Figure 8. Validation of the 60 gsm based ERV: (a) Sensible, (b) Latent.

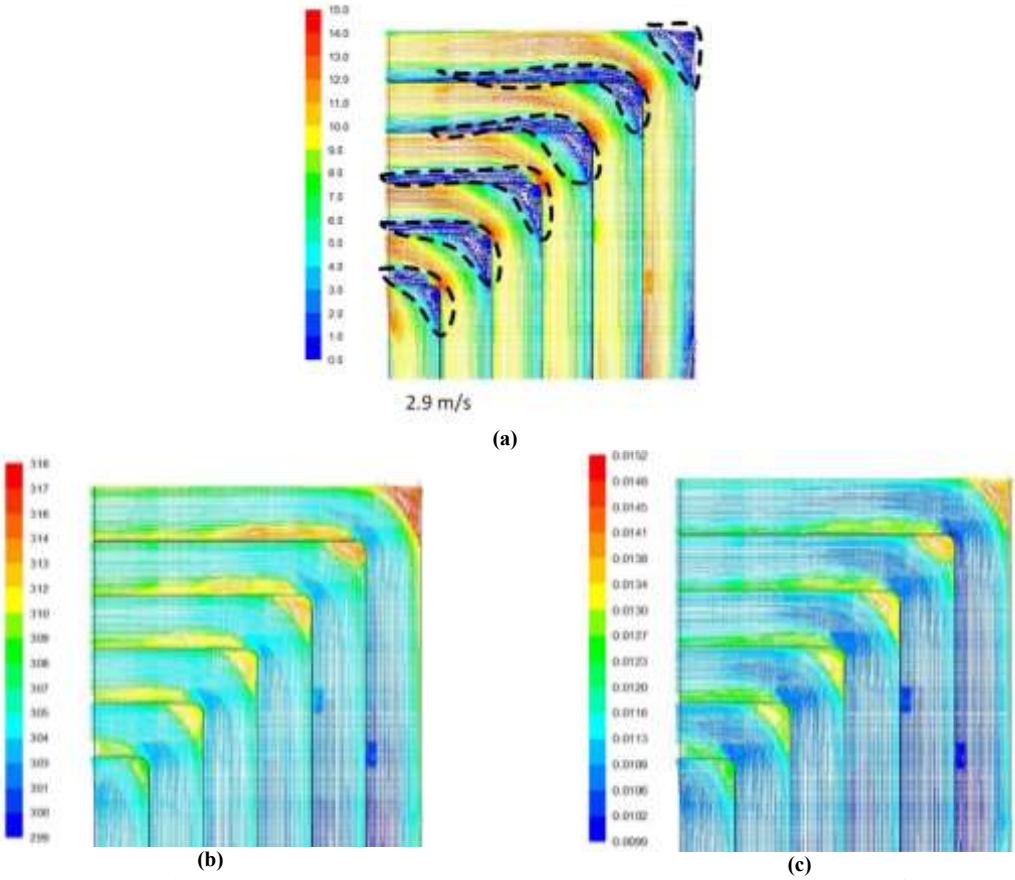

(a)

(b) (c)

Figure 9. Velocity vectors showing circulation zones within the ERV and colored by: (a) velocity magnitude (m/s), (b) air temperature (K), (c) vapor mass fraction (kgv/kg).

The dependence of effectiveness on the face velocity is clear throughout the study. As the velocity increases, the effectiveness decreases. This could be related to the residence time of hot and cold streams within the ERV. Lower velocity means more time for the heat and mass exchange between the two streams leading to higher effectiveness. Higher velocity means less time and lower effectiveness that resulted from flow circulation within the ERV as shown by Figure 9.The zones circulated by dashed lines represent the zones that contain air circulation. From Figure 9a, the air speed dropped to less than 1 m/s within the circulation zone and increased to almost 14 m/s at the channel separators outside corners. Apparently, the corners of the ERV separators were not streamlined for such high velocity which enhanced the occurrence of air circulation

Figure **11** show the effect of the adopted turbulence model of the distribution of mass fraction values with the given air stream. It is worth mentioning that the simulated cases had different inlet conditions of air temperatures, mass fractions and face velocities as detailed in Figure 10. Furthermore, the presented values reflect a counter flow profile that are located at the center of the ERV.

The simulated k-ε models have shown little variations in predicting the mass fraction values at all Re values. However, there were differences in predicting the mass fraction values when compared to the SST k-ω turbulence model. The difference is clear at low Re values and starts to diminish as Re values increased towards the fully developed turbulent flow values. At low Re value of 1278, it has been found that the difference in mass fraction values at both sides of the membrane is equal to 0.00084 and 0.00094 kgv/kg for k-ε models and SST k-ω model, respectively.

The max difference value of 0.0051 kgv/kg that does exist at the inlets of ERV channels. This demonstrates that the SST k-ω model shows more sensitivity towards the low Re value that enhance the diffusion across the membrane which is reflected on low values of mass fraction at the hot stream and high values at the cold stream. The expected higher performance of mass transfer and energy recovery at low Re values is better demonstrated by the SST k-ω model when compared to the k-ε simulated models. At Re = 2253, all simulated models showed similar behavior of predicting the mass fraction values with similar driving force for mass transfer across the membrane of 0.00058 kgv/kg. the mass fraction profile away from the membrane surface was also similar for all simulated models. The difference in predicting the mass fraction reappeared at Re values of 4119 and 4859 with the SST k-ω model predicting less mass transfer values than the k-ε simulated models.

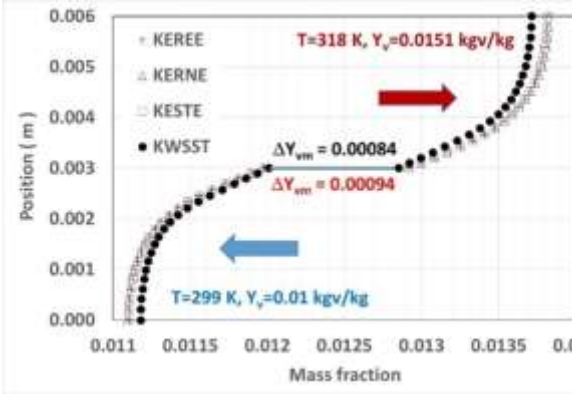

behavior. Effects of the air circulation on the thermal/moist exchange between the two streams is shown by Figure 9b at the symmetry surface of the cold stream. The air temperature within the circulation zones were higher than outside the zones due to lower air speed. The vapor mass fraction behaved similar to air temperature as shown by Figure 9c.

The main advantage of the utilized UDF is the prediction of mass fraction values at both sides of the membrane that are in touch with hot and cold streams. Based on the value of the mass fraction of moist air adjacent to the membrane surface, the UDF predicted the mass fraction value that needs to be given as a boundary condition at the given hot or cold sides of the membrane. Figure 10 and

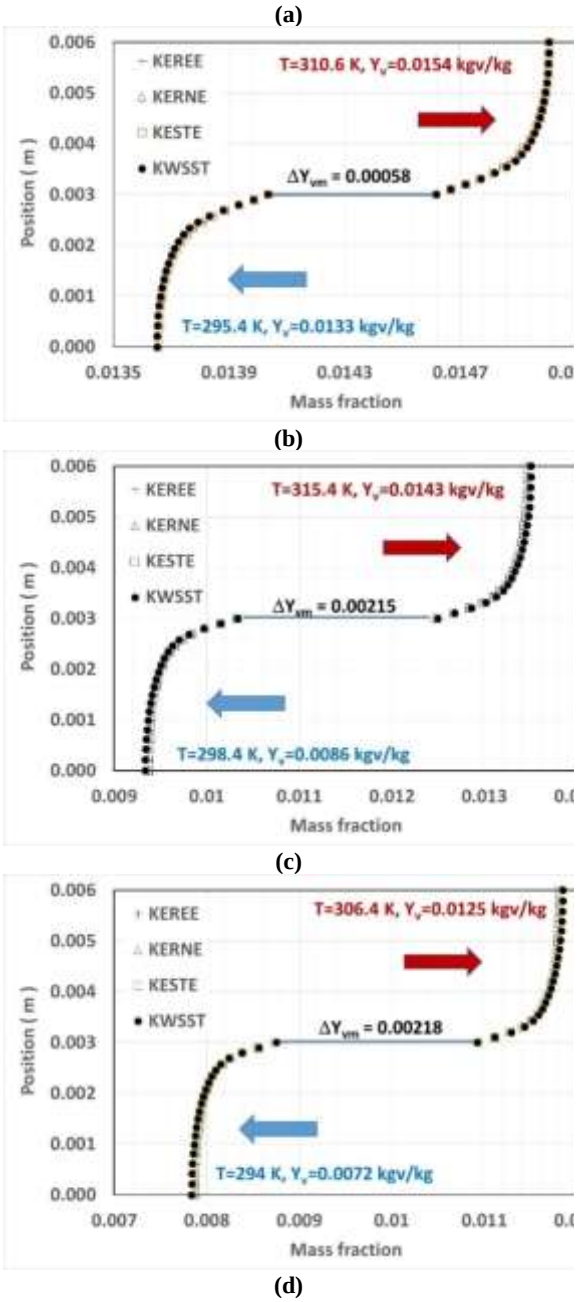

Figure 10. Mass fraction profile within hot and cold channels at different Re values: (a) 1278, (b) 2253, (c) 4119 , (d) 4859 .

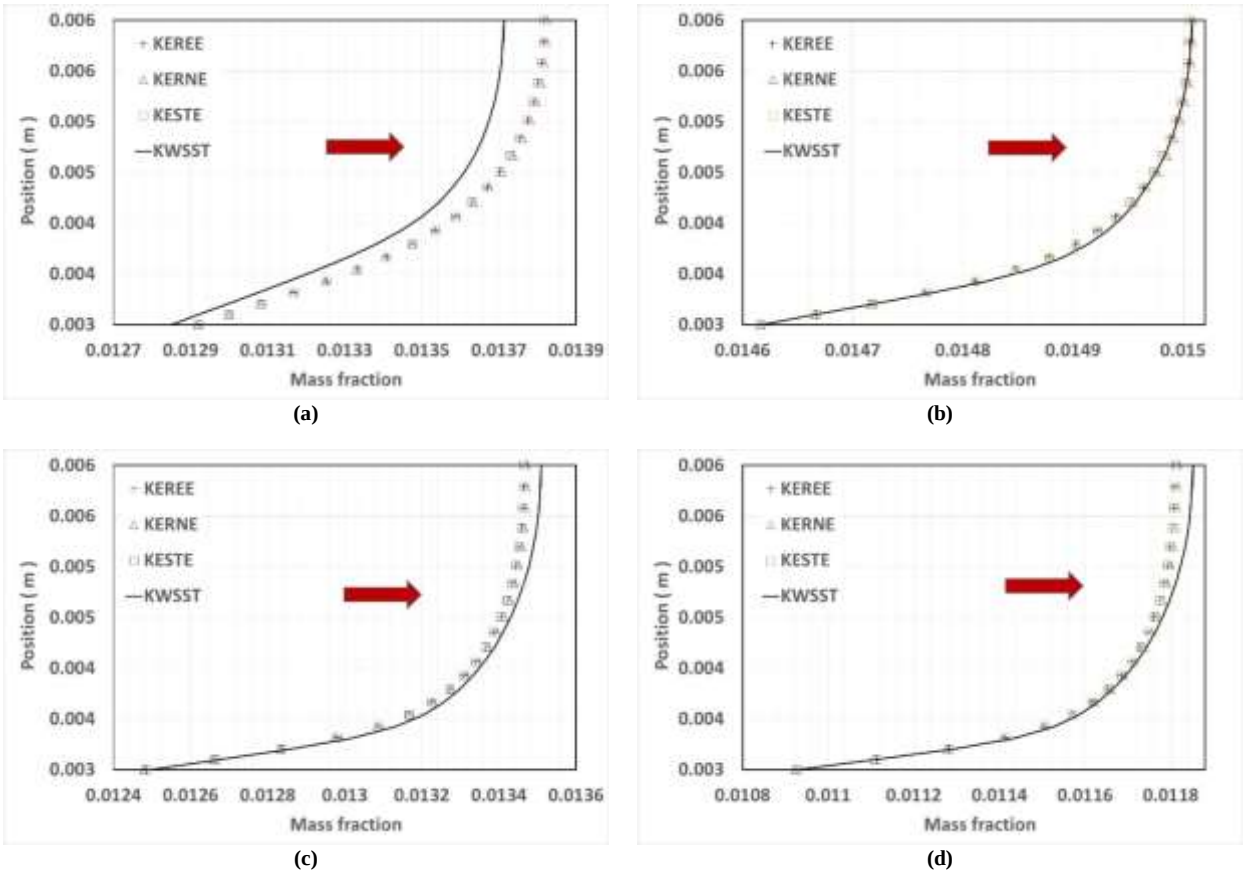

Figure 11. Differences in mass fraction profiles within hot channels as a function of simulated turbulence models at different Re values: (a) 1278, (b) 2253, (c) 4119, (d) 4859.

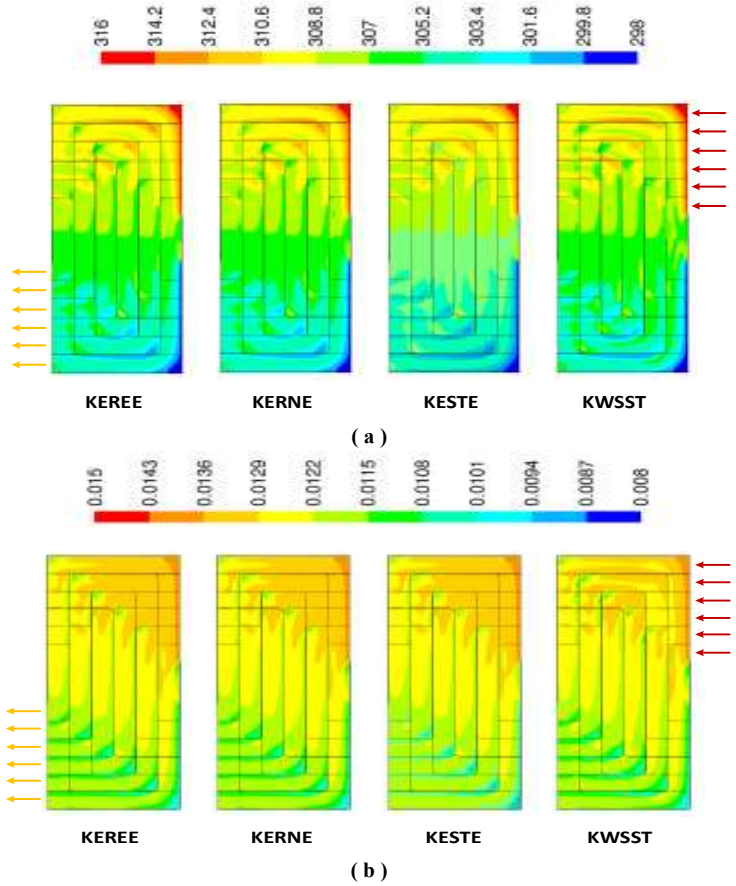

Figure 12. Colored contours for Re = 4119 cases at the hot side surface of the membrane: (a) Temperature (K); (b) Mass fraction (kgv/kg).

All simulated models showed similar predictions at cells close to the membrane surfaces which could be seen clearly from Figure 12and slight differences at the symmetry surface as shown by Figure 13. This is due to the relatively high Re value of 4119 which is considered a developing turbulent flow and the turbulent wall treatment is considered effective. The effect of circulation zones is evident where spots of low/high temperature and mass fraction values appeared around the corners of air flow channels which confirm the finding presented earlier by Figure 9. At the symmetry surface a difference has been noticed for the case of SST k-ω model. The high values of temperature and mass fraction at the hot stream of flow covers more area for the SST k-ω model in comparison with the other simulated models. Similar notes could be made regarding the circulation zones and lower values of temperature and mass fraction due to more residence times that enhanced the heat and mass transfer process across the membrane.

3.3. Case study: MENA Region

The MENA region is well known for its hot summer and diverse winter climates. Table 2 lists the design conditions for the investigated cities within the MENA region based on ASHRAE weather conditions. The Gulf states possessed the highest ambient air temperature which is expected to affect the sensible load of HVAC system. However, Karachi and Beirut produced the highest enthalpy conditions which is expected to affect the total load of the coil. The investigated cities produced enthalpies higher than the air-conditioned space enthalpy at design conditions.

In order to demonstrate the suitability of the examined ERV, a typical open area office of 200 m^2 space was adopted to the current simulations using HAP software [49]. The HVAC system utilized was a packaged rooftop unit with aconstant air volume (CAV) system as depicted by Figure 14. The static pressure of the utilized supply fan was assumed to be 500 Pa. furthermore, additional static pressure was utilized when the ERV was running and the exhaust fan was utilized.

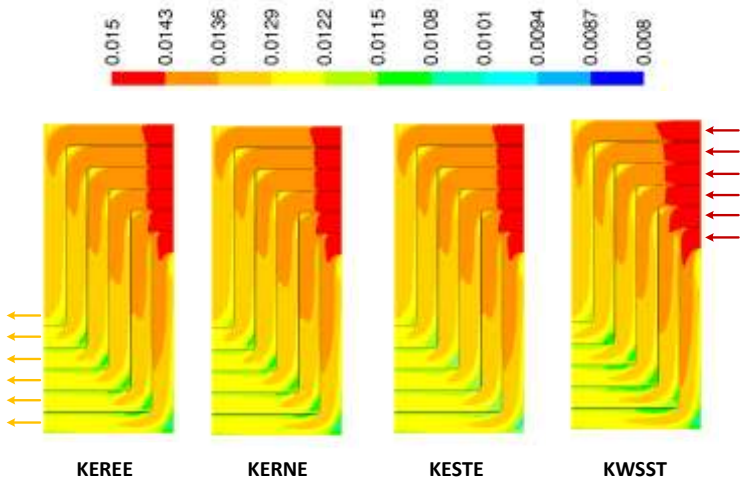

(b)

Figure 13. Colored contours for Re = 4119 cases at the hot side symmetry surface: (a) Temperature (K), (b) Mass fraction (kgv/kg).

Table 2. Reference values of the worldwide modelled cities with different climate zones.

City	Cooling			Heating		
	Dry Bulb (°C)	Wet Bulb (°C)	Enthalpy (kJ/kg)	Dry Bulb (°C)	Wet Bulb (°C)	Enthalpy (kJ/kg)
Design Room	24.0	17.1	47.00	21.0	13.0	36.5
Amman, Jordan	35.0	18.3	51.40	0.6	-2.5	5.5
Manama, Bahrain	39.8	25.0	75.82	11.1	6.4	21.4
Baghdad, Iraq	45.0	22.8	66.74	0.0	-2.8	5.0
Kuwait, Kuwait	47.2	20.6	58.62	3.3	-0.1	9.7
Beirut, Lebanon	32.8	25.6	78.72	5.6	1.8	12.6
Karachi, Pakistan	37.8	27.8	88.51	9.4	5.1	18.8
Doha, Qatar	42.8	21.7	62.72	10.6	6.0	20.6
Riyadh, KSA	43.9	17.8	49.53	5.0	1.2	11.6
Abu Dhabi, UAE	43.9	23.3	68.73	11.1	6.4	21.4
Cairo, Egypt	37.8	20.6	58.98	7.2	3.2	15.2
Rabat, Morocco	32.8	23.9	71.59	4.4	0.8	10.9
Tunis, Tunisia	36.7	22.8	67.09	5.0	1.3	11.7

The first step in the current study was to estimate the outdoor requirement for the adopted HVAC system and to size the required cooling/heating coils. Figure 15 shows the air flow rates requirements based on the simulated city. The supplied air requirement ranged from 3519 L/s for Rabat to 4433 L/s for Riyadh with the remaining cities located in between. These amounts of air are required to provide the comfortable conditions within the air-conditioned office in terms of temperature, humidity and CO_2 concentration. Under the basic case of no ERV utilization, the percentage of outdoor air requirements to the supplied air is shown by Figure 15b. It can be seen that the resulted percentage was between 5.5% and 7% based on providing 8 L/s per person. Installing an ERV unit based on the low percentage is not feasible. It is well known that increasing the amount of outdoor air per person will increase the feeling of comfort and productivity. Therefore, a study has been conducted on the feasibility of providing outdoor air with flowrate equal to 30% of the supplied air. The resulted quantities are shown by Figure 15a for each city. For these scenarios, the estimated coil sizes and electrical energy consumption were simulated on annual basis.

The total coil load of the HVAC system with and without the ERV unit was estimated and shown by Figure 16. In the MENA region the HVAC system peak load sizing is based on the cooling coil size rather than the heating coil size as shown. The basic case of no ERV and lowest ventilation rate resulted in the lowest coil size with values ranging from 40 kW for Amman to 52 kW for Kuwait and Karachi. The biggest coil size resulted from providing 30% of the supplied air from outdoor with values ranging from 52 kW for Amman and 90 kW for Karachi. The effect of higher outdoor enthalpy is clear from the obtained results were Karachi demands for cooling outperformed the high temperatures of the Gulf region. Therefore, high outdoor temperature alone is not necessarily leading to bigger coil size. It is the outdoor enthalpy, that include effects of both temperature and humidity, that dictate the coil size. The total coil size with the ERV unit installed has resulted in average values between the basic case and the 30% ratio case with values ranged from 43 kW for Amman and 59 kW for Karachi. This remains higher than the basic case but at a better indoor air quality for enhanced productivity and lower sick building syndrome possibility.

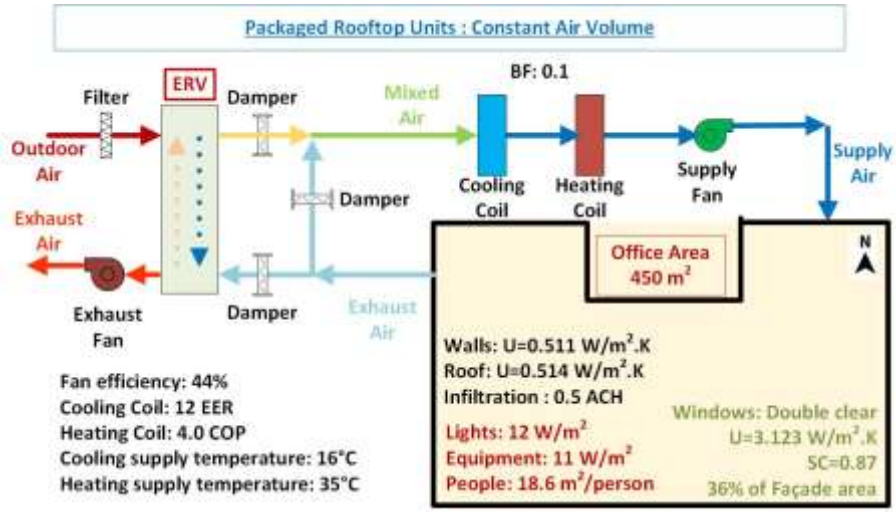

Figure 14. General view of the utilized HVAC system.

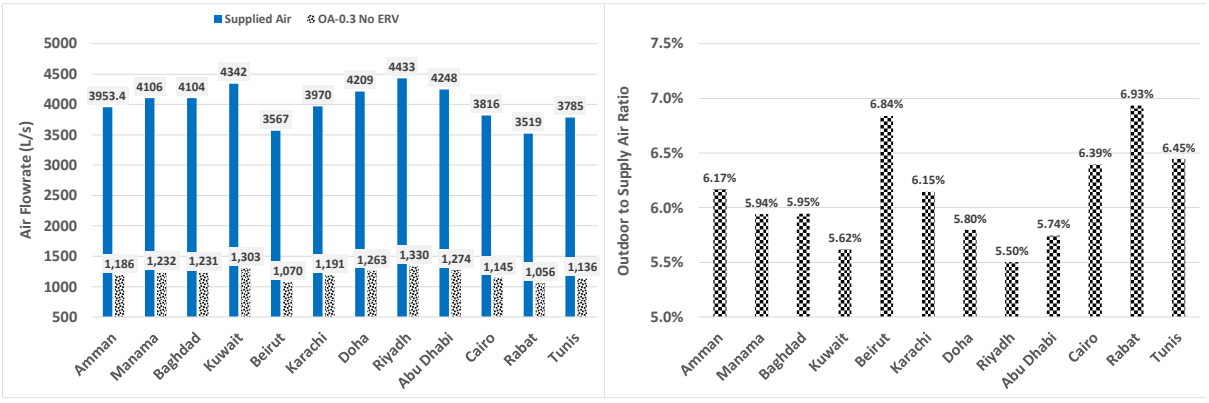

(a) **(b)**

Figure 15. Air flow rates requirement: (a) amount of supplied air and the 30% of outdoor air; (b) percentage of outdoor air to supply air without ERV utilization

The installation of the ERV unit at the 30% outdoor to supply air ratio has resulted in coil downsizing as shown by Figure 16b. It is clear that the ERV unit performs better at high outdoor humidity and temperature as in the case of Karachi with cooling coil downsizing of about 31 kW. For Amman, Cairo and Tunis the performance of ERV in winter time outperformed the performance in summer time resulting in greater heating coil downsizing than cooling coil downsizing. For Baghdad and Rabat, the ERV unit performed similarly during summer and winter times. For the remaining cities, the ERV unit was a positive advantage during the summer time with cooling coil downsizing values from 18 kW for Abu Dhabi to around 22 kW for Kuwait.

The downsizing resulted from installing the ERV unit contributes to the initial cost of the HVAC system. The running cost could be represented by how much electrical energy saved as a result of the ERV unit utilization. Figure 17 shows the amount of electrical energy saved and the percentage of the total operating electrical energy of the HVAC system. Similar trends were found to those of the cold downsizing were Amman and Tunis resulted in the highest percentage of electrical energy savings (11%) due to their relatively small coil sizes and the high performance in winter times. In cities with high cooling demands around the year the saving was less and the overall percentage was around 5%.

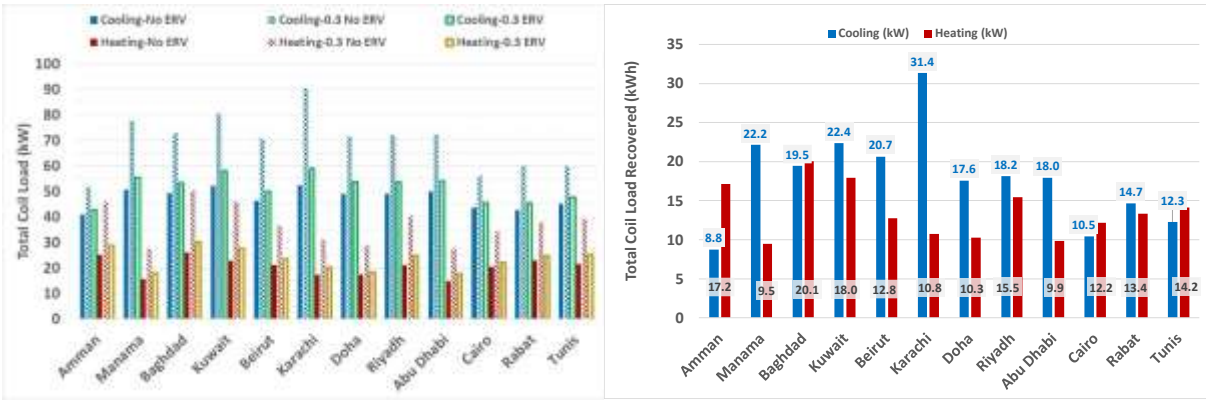

(a) **(b)**

Figure 16. Comparison of total coil loads: (a) under different outdoor air and ERV strategies; (b) Coil downsizing as a result of utilizing the ERV unit.

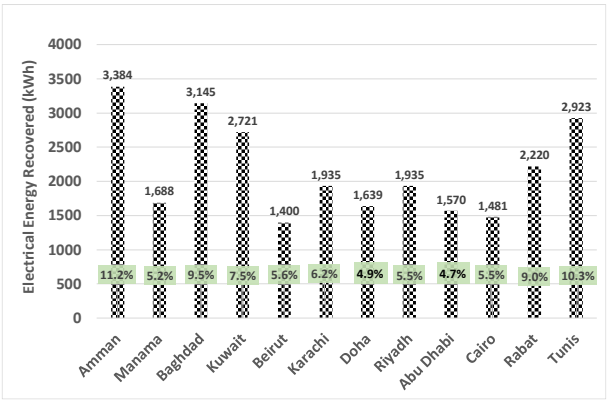

(a)

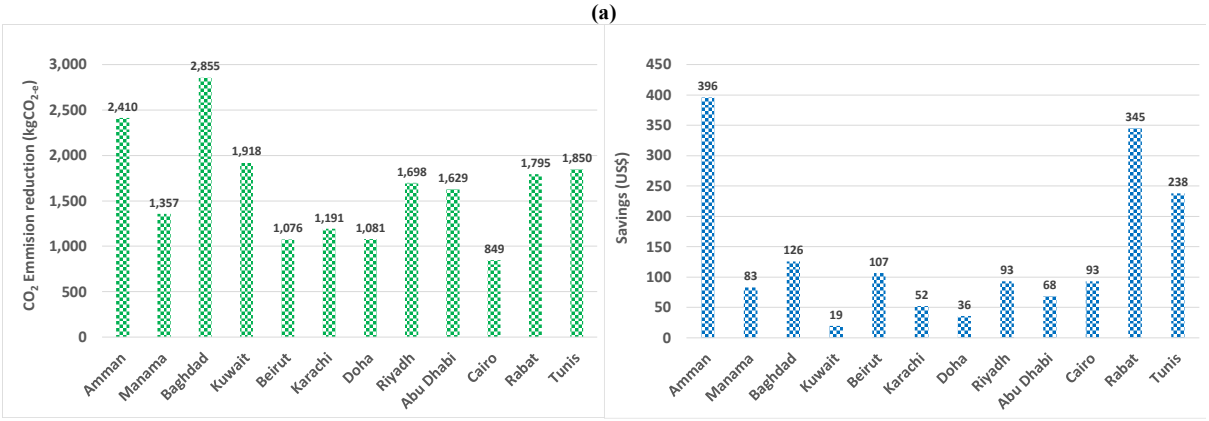

(b) **(c)**

Figure 17. Annual savings due to ERV utilization: (a) electrical energy consumption; (b) CO2 emissions; (c) running cost.

This could be due to the big coil size of the HVAC system that resulted in lower percentage. The reduction in electrical energy consumption could be reflected on the reduction of CO_2 emissions and savings in the running cost as shown by Figure 17b and Figure 17c. Annual reduction in CO_2 emissions due to the installation of the ERV unit could reach upto 2,855 kgCO_2-e for Baghdad and as low as 849 kgCO_2-e for Cairo. These are significant figures and contribute to a much healthier environment. The annual running cost savings ranged from US$19 for Kuwait to US$386 for Amman. The price of electricity played a major factor in getting these figures. The highly subsidized electricity prices in the Gulf region, Cairo and Karachi contributed to the low savings in the running cost of the HVAC system. However, the savings in running cost for Amman, Rabat and Tunis were significant. In an overall evaluation, the utilization of ERV units in the MENA region could be considered as an added value of success to office buildings HVAC systems.

The performance of theHVAC system was presented without specification towards the performance of the ERV unit alone. Figure 18 shows the ratio of energy recovery (RER) performance parameter of the utilized ERV across the MENA region. As expected, the ERV was least performed in cities under the effect Mediterranean climate due to relatively moderate temperatures and humidity with RER values between 31 and 44. Under the extreme temperatures of the hot and arid climates of Baghdad and Riyadh, the RER values were between 51 and 55. The most suitable climate for the utilization of an ERV unit is the tropical/semitropical climate with coastal cities. That was the results obtained for Gulf cities apart from Riyadh and for Karachi which is located at the coast of Arabian sea with RER values between 68 and 93. The hot and humid weather of Manama made it the most suitable city for the ERV to perform. It can be concluded, that ERV units are a necessary element in any HVAC system in the era of energy efficient systems and green buildings.

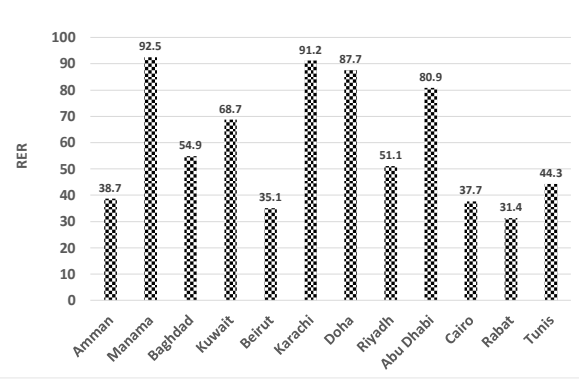

Figure 18. Performance of the ERV at different locations within the MENA region.

4. Conclusions

The tradition practice in HVAC system in office building was to minimize the outdoor air into the system in order to lower the running cost. The ERV units have given an opportunity to HVAC systems designers to provide a comfortable and more productive environment at and acceptable cost. The 60 gsm paper membrane based ERV performance under four turbulence models: laminar model, Standard k-ε, RNG k-ε, realizable k-ε and SST k-ω was simulated. Energy transfer inside the ERV, across the paper membrane, were modelled numerically using Ansys® Fluent v18.1 and adopting a specially developed UDF. The following conclusions are made:

- Mesh sensitivity analysis revealed that lateral distance of the mesh elements is not as significant as the perpendicular distance from the membrane surface. Under turbulence modelling, a fine mesh must be used with perpendicular distances less than the membrane thickness and must meet the condition of $y^+ \approx 1$.
- The assumption of linear and laminar profiles of the mass fraction distribution proved to be valid at all investigated face velocities. Furthermore, the simulated turbulence models behaved similarly in predicting the ERV performance due the relatively low Re where the separation and circulation effects on the turbulent flow are not strong enough to cause major differences.
- The SST k-ω showed greater sensitivity to the nature of flow structure at different Re values when compared with Standard k-ε, RNG k-ε, realizable k-ε turbulence models. Therefore, the SST k-ω model is preferable to be used for simulating turbulent flow within a given membrane ERV.
- ERV technology is optimal for the HVAC industry in Jordan where it provides better indoor air quality and comfortable and energy efficient HVAC systems. A TER value of 38 W per channel at 0.76 m/s face velocity could be obtained and it could reach 100 W at 2.66 m/s face velocity. This comes at an additional pressure drop of 220 Pa at 2.66 m/s face velocity.
- High outdoor temperature and humidity provide a better environment for the utilization of ERV units with RER values for the MENA region ranging between 31 and 93 at a minimum of 30% of outdoor air quantity in the supply air.The ERV unit could results in upto 11% savings of electrical energy under the Mediterranean climate and upto 5% under the Gulf climate.
- The performance of ERV in winter time could outperformed the performance in summer time under the Mediterranean climate. A maximum cooling coil downsizing of up to 31 kW was achieved for Karachi city and a minimum of around 9 kW was achieved for Amman city. Savings in annual running cost for the HVAC systems of upto US$386 could be achieved for Amman.

Acknowledgments

The current work has utilized equipment that was supported by the Deanship of Scientific Research of GJU under Seed Grant Number (SATS 06/2018).

References

[1] Xu Q., Riffat S., Zhang S., Review of Heat Recovery Technologies for Building Applications, Energies, 12 (7) (2019) 1285.

[2] Alshorman A.A., Alrawashdeh K.A., Alshorman M., Talat N.T., Validation of jordanian green building based on LEED standard for energy efficiency methodology, Jordan Journal of Mechanical and Industrial Engineering, 12 (2018) 51-58.

[3] Al-Widyan M.I., Soliman I.A., Alajlouni A.A., Al Zu'bi O.I., Jaradat A.I., Energy performance assessment of a non-domestic service building in Jordan, Jordan Journal of Mechanical and Industrial Engineering, 12 (2) (2018) 69-75.

[4] Jarada H., Ashhab M.S., Energy savings in the Jordanian residential sector, Jordan Journal of Mechanical and Industrial Engineering, 11 (1) (2017) 51-59.

[5] Mardiana-Idayu A., Riffat S.B., Review on heat recovery technologies for building applications, Renewable and Sustainable Energy Reviews, 16 (2) (2012) 1241-1255.

[6] ASHRAE, ASHRAE Handbook: HVAC Systems and Equipment, American Society of Heating, Refregirating and Air Conditioning Engineers, Inc., Atlanta, GA, 2016.

[7] Sabek S., Tissb F., Chouikhab A., Guizani R., Numerical investigation of heat and mass transfer in partially blocked membrane-based heat exchanger: Effects of obstacles forms, Applied Thermal Engineering, 130 (2018) 211-220.

[8] M.M. Aslam Bhutta, N. Hayat, M.H. Bashir, A.R. Khan, K.N. Ahmad, S. Khan, CFD applications in various heat exchangers design: A review, Applied Thermal Engineering, 32 (2012) 1-12.

[9] Saraireh M., Computational fluid dynamics simulation of plate fin and circular pin fin heat sinks, Jordan Journal of Mechanical and Industrial Engineering, 10 (2016) 99-104.

[10] Gawande V.B., Dhoble A.S., Zodpe D.B., Chamoli S., A review of CFD methodology used in literature for predicting thermo-hydraulic performance of a roughened solar air heater, Renewable and Sustainable Energy Reviews, 54 (2016) 550-605.

[11] A. Kumar, J.B. Joshi, A.K. Nayak, A comparison of thermal-hydraulic performance of various fin patterns using 3D CFD simulations, International Journal of Heat and Mass Transfer, 109 (2017) 336-356.

[12] S.R. Shabanian, M. Rahimi, M. Shahhosseini, A.A. Alsairafi, CFD and experimental studies on heat transfer enhancement in an air cooler equipped with different tube inserts, International Communications in Heat and Mass Transfer, 38 (3) (2011) 383-390.

[13] Li M., Khan T.S., Al-Hajri E., Ayub Z.H., Single phase heat transfer and pressure drop analysis of a dimpled enhanced tube, Applied Thermal Engineering, 101 (2016) 38-46.

[14] Ozden E., Tari I., Shell side CFD analysis of a small shell-and-tube heat exchanger, Energy Conversion and Management, 51 (5) (2010) 1004-1014.

[15] Chaube A., Sahoo P.K., Solanki S.C., Effect of roughness shape on heat transfer and flow friction characteristics of solar air heater with roughend absorber plate, WIT Transactions of Engineering Science, 53 (2006) 43-51.

[16] E. Pal, I. Kumar, J.B. Joshi, N.K. Maheshwari, CFD simulations of shell-side flow in a shell-and-tube type heat exchanger with and without baffles, Chemical Engineering Science, 143 (2016) 314-340.

[17] Hatami M., Jafaryar M., Ganji D.D., Gorji-Bandpy M., Optimization of finned-tube heat exchangers for diesel exhaust waste heat recovery using CFD and CCD techniques, International Communications in Heat and Mass Transfer, 57 (2014) 254-263.

[18] Sharma S.K., Kalamkar V.R., Computational Fluid Dynamics approach in thermo-hydraulic analysis of flow in ducts with rib roughened walls – A review, Renewable and Sustainable Energy Reviews, 55 (2016) 756-788.

[19] Taler D., Ocłoń P., Thermal contact resistance in plate fin-and-tube heat exchangers, determined by experimental data and CFD simulations, International Journal of Thermal Sciences, 84 (2014) 309-322.

[20] Kanaris A.G., Mouza A.A., Paras S.V., Flow and heat transfer in narrow channels with corrugated walls a cfd code application, Chemical Engineering Research and Design, 83 (2005) 460-468.

[21] Nasif M.S., Analysis and Modelling of Membrane Heat Exchanger in HVAC Energy Recovery Systems, PhD Thesis in Mechanical Engineering, University of New South Wales, 2006.

[22] Nasif M.S., Effect of utilizing different permeable material in air-to-air fixed plate energy recovery heat exchangeron energy saving, ARPN Journal of Engineering and Applied Sciences, 10 (21) (2015) 10153-10158.

[23] Nasif M.S., Al-Waked R., Behnia M., Morrison G., Air to air enthalpy heat exchanger, Heat Transfer Engineering, 33 (12) (2012) 1010-1023.

[24] Nasif M.S., Al-Waked R., Behnia M., Morrison G., Air to air fixed plate enthalpy heat exchanger, performance variation and energy analysis Journal of Mechanical Science and Technology, 27 (11) (2013) 3541-3551.

[25] Nasif M.S., Al-Waked R., Morrison G., Behnia M., Membrane heat exchanger in HVAC energy recovery systems: systems energy analysis, Energy and Buildings, 42 (2010) 1833-1840.

[26] Nasif M.S., Al-Waked R., Ismail F., Numerical investigation on the effect of varying the number of flow dividers on Z-Shaped membrane heat exchanger performance Malaysian Journal of Fundamental and Applied Sciences, 16 (1) (2020) 85-89.

[27] Al-Waked R., Bani Mostafa D., Nasif M.S., Performance of energy recovery ventilators under different climatic regions, Energy Efficiency, 14 (1) (2021) 8.

[28] Al-Waked R., Nasif M.S., Air to air energy recovery from HVAC systems under different membrane materials, Universal Journal of Mechanical Engineering, 7 (2) (2019) 37-49.

[29] Xu J., Zhang C., Ge T., Dai Y., Wang R., Performance study of sodium alginate-nonwoven fabric composite membranes for dehumidification, Applied Thermal Engineering, 128 (2018) 214-224.

[30] Lekshminarayanan G., Croal M., Maisonneuve J., Recovering latent and sensible energy from building exhaust with membrane-based energy recovery ventilation, Science and Technology for the Built Environment, 26 (7) (2020) 1000-1012.

[31] Albdoor A.K., Ma Z., Cooper P., Experimental investigation and performance evaluation of a mixed-flow air to air membrane enthalpy exchanger with different configurations, Applied Thermal Engineering, 166 (2020) 114682.

[32] Baldinelli G., Rotili A., Narducci R., Di Vona M.L., Marrocchi A., Experimental analysis of an innovative organic membrane for air to air enthalpy exchangers, International Communications in Heat and Mass Transfer, 108 (2019) 104332.

[33] Zhang L.Z., Heat and mass transfer in a cross-flow membrane-based enthalpy exchanger under naturally formed boundary conditions, International Journal of Heat and Mass Transfer, 50 (2007) 151-162.

[34] Zhang L.Z., Heat and mass tansfer in a quasi-counterflow membrane-based total heat exchanger, International Journal of Heat and Mass Transfer, 53 (2010) 5478-5486.

[35] Al-Waked R., Nasif M.S., Morrison G., Behnia M., CFD simulation of air to air enthalpy heat exchanger, Energy Conversion and Management, 74 (2013) 377-385.

[36] Al-Waked R., Nasif M.S., Morrison G., Behnia M., CFD simulation of air to air enthalpy heat exchanger: Variable membrane moisture resistance, Applied Thermal Engineering, 84 (6) (2015) 301-309.

[37] W. Yaïci, M. Ghorab, E. Entchev, 3D CFD study of the effect of inlet air flow maldistribution on plate-fin-tube heat exchanger design and thermal–hydraulic performance, International Journal of Heat and Mass Transfer, 101 (2016) 527-541.

[38] Yaïci W., Ghorab M., Entchev W., Numerical analysis of heat and energy recovery ventilators performance based on CFD

for detailed design, Applied Thermal Engineering, 51 (1-2) (2013) 770-780.
[39] Sebai R., Chouikh R., Guizani A., Cross-flow membrane-based enthalpy exchanger balanced and unbalanced flow, Energy Conversion and Management, 87 (2014) 19-28.
[40] Deshko V.I., Karvatskii A.Y., Sukhodub I.O., Heat and mass transfer in cross-flow air-to-air membrane heat exchanger in heating mode, Applied Thermal Engineering, 100 (2016) 133-145.
[41] Sabek S., Tiss F., Chouikh R., Guizani A., Numerical investigation of membrane based heat exchanger with partially blocked channels, Applied Thermal Engineering, 104 (2016) 203-211.
[42] Nam S.H., Han H., Computational modeling and experimental validation of heat recovery ventilator under partially wet conditions, Applied Thermal Engineering, 95 (2016) 229-235.
[43] Kroger D.K., Air-Cooled heat exchangers and cooling towers, PennWell Corp., Tulsa, USA, 2004.
[44] Cengel Y.A., Heat and mass transfer: A practical approach, Third ed., McGraw-Hill, Singapor, 2006.
[45] Launder B.E., Spalding D.B., The Numerical Computation of Turbulent Flow, Computer Methods in Applied Mechanics and Engineering, 3 (1974) 269-289.
[46] Orszag S.A., Yakhot V., Flannery W.S., Boysan F., Choudhury D., Maruzewski J., Patel B., Renormalization Group Modeling and Turbulence Simulations, in: International Conference on Near-Wall Turbulent Flows, Tempe, Arizona, , 1993.
[47] Shih T.H., Liou W.W, Shabbir A., Yang Z., Z. J.. A new - eddy-viscosity model for high reynolds number turbulent flows - model development and validation, Computers & Fluids, 24 (3) (1995) 227-238.
[48] Menter F.R., Two-Equation Eddy-Viscosity Turbulence Models for Engineering Applications, AIAA Journal, 32 (8) (1994) 1598-1605.
[49] Carrier, Hourly analysis program (HAP v4.9) quick reference guide, 8th edition ed., Carrier Corporation, 2014.